Association of α-Synuclein and Mutants with Lipid Membranes: Spin-Label ESR and Polarized IR†

Muthu Ramakrishnan,‡ Poul H. Jensen,§ and Derek Marsh*,‡

Max-Planck-Institut für biophysikalische Chemie, Abt. Spektroskopie, 37070 Göttingen, Germany, and University of Aarhus, Institute of Medical Biochemistry, 8000 Aarhus C, Denmark

Received November 16, 2005; Revised Manuscript Received January 6, 2006

ABSTRACT: α-Synuclein is a presynaptic protein, the A53T and A30P mutants of which are linked independently to early-onset familial Parkinson's disease. The association of wild-type α-synuclein with lipid membranes was characterized previously by electron spin resonance (ESR) spectroscopy with spin-labeled lipids [Ramakrishnan, M., Jensen, P. H., and Marsh, D. (2003) *Biochemistry 42*, 12919−12926]. Here, we study the interaction of the A53T and A30P α-synuclein mutants and a truncated form that lacks the acidic C-terminal domain with phosphatidylglycerol bilayer membranes, using anionic phospholipid spin labels. The strength of the interaction with phosphatidylglycerol membranes lies in the order: wild type ≈ truncated > A53T > A30P > fibrils ≈ 0, and only the truncated form interacts with phosphatidylcholine membranes. The selectivity of the interaction of the mutant α-synucleins with different spin-labeled lipid species is reduced considerably, relative to the wild-type protein, whereas that of the truncated protein is increased. Polarized infrared (IR) spectroscopy is used to study the interactions of the wild-type and truncated proteins with aligned lipid membranes and additionally to characterize the fibrillar form. Wild-type α-synuclein is natively unfolded in solution and acquires secondary structure upon binding to membranes containing phosphatidylglycerol. Up to 30−40% of the amide I band intensity of the membrane-bound wild-type and truncated proteins is attributable to β-sheet structure, at the surface densities used for IR spectroscopy. The remainder is α-helix and residual unordered structure. Fibrillar α-synuclein contains 62% antiparallel β-sheet and is oriented on the substrate surface but does not interact with deposited lipid membranes. The β-sheet secondary-structural elements of the wild-type and truncated proteins are partially oriented on the surface of membranes with which they interact.

α-Synuclein is a soluble presynaptic protein that is involved in several forms of neurodegenerative disease (for a review, see ref *1*). It is the major component of the pathological lesions associated with Parkinson's disease, the Lewy body variant of Alzheimer's disease, dementia with Lewy bodies, Down's syndrome, and multiple system atrophy. Significantly, three missense mutations of α-synuclein are linked genetically with familial early-onset Parkinson's disease (*2*, *3*) and additionally with Lewy body dementia (*4*).

Although a cytosolic protein, α-synuclein has been found to bind to membranes containing negatively charged lipids (*5*−*8*). It is therefore likely that association with the membrane may be involved in both the normal and pathogenic function of α-synuclein, because association of cellular α-synuclein with lipid droplets results in the formation of small oligomers that may be precursors of larger aggregates (*9*). This suggestion is supported by the fact that the N-terminal domain (residues 1−102) of the protein contains seven 11-residue repeats of consensus sequence pKTKEGVaxaA, where p is a polar residue, a is an apolar residue, and x is any residue (*6*, *10*). Such a motif characterizes class A_2 amphipathic helices that are found in the lipid-binding domains of exchangeable serum apolipoproteins (*11*). NMR studies have confirmed that it is only this repeat region of α-synuclein that is bound to lipids or detergent micelles (*12*, *13*). Furthermore, α-synuclein and its prefibrillar oligomers have been found capable of permeabilising vesicles composed of negatively charged phospholipids (*14*, *15*).

Previously, we have used chain-labeled phospholipid electron spin resonance (ESR)[1] probes to characterize the interactions of wild-type α-synuclein with lipid bilayer membranes (*16*). In the present work, we use this method to study the interaction of the two disease-related mutants, A53T and A30P, of α-synuclein and a truncated form that lacks the acidic C-terminal domain, with phosphatidylglycerol and phosphatidylcholine membranes. Complementary

† M.R. is a recipient of an Alexander-von-Humboldt Fellowship.

* To whom correspondence should be addressed: Max-Planck-Institut für biophysikalische Chemie, Abt. Spektroskopie, 37070 Göttingen, Germany; tel.: +49−551−201 1285; fax: +49−551 201 1501; e-mail: dmarsh@gwdg.de.

‡ Max-Planck-Institut für biophysikalische Chemie.

§ University of Aarhus.

[1] Abbreviations: DMPG, 1,2-dimyristoyl-*sn*-glycero-3-phosphoglycerol; DMPC, 1,2-dimyristoyl-*sn*-glycero-3-phosphocholine; 5-SASL, 5-(4,4-dimethyloxazolidine-*N*-oxyl)stearic acid; 5-PGSL, -PCSL, -PESL, -PASL, -PSSL, 1-acyl-2-[5-(4,4-dimethyloxazolidine-*N*-oxyl)]stearoyl-*sn*-glycero-3-phosphoglycerol, -phosphocholine, -phosphoethanolamine, phosphatidic acid, -phosphoserine; 5-DGSL, 1-acyl-2-[5-(4,4′-dimethyloxazolidine-*N*-oxyl)]stearoyl-*sn*-glycerol; 5-NAPESL, 1,2-dipalmitoyl-*sn*-glycero-3-[*N*-5-(4,4-dimethyloxazolidine-*N*′-oxyl)stearoyl]-phosphoethanolamine; Hepes, *N*-(2-hydroxyethyl)piperazine-*N*′-2-ethanesulphonic acid; EDTA, ethylenediaminetetraacetic acid; ESR, electron spin resonance; IR, infrared; ATR, attenuated total reflectance.

10.1021/bi052344d CCC: $33.50
Published on Web 02/08/2006

studies, with polarized infrared (IR) spectroscopy, are used to characterize the conformation and orientation of the wild-type, mutant, and truncated proteins interacting with aligned lipid membranes and additionally to investigate the fibrillar form of α-synuclein.

MATERIALS AND METHODS

Materials. The following recombinant human α-synuclein proteins were expressed and purified as previously described: wild-type α-synuclein(1−140) (*17*), the A30P and A53T α-synuclein mutants (*18*), and the C-terminally truncated α-synuclein(1−95) (*19*). The purified proteins were lyophilised using a SpeedVac (Savant). α-Synuclein fibrils assembled from wild-type α-synuclein were prepared and purified from nonaggregated α-synuclein by sucrose density-gradient centrifugation as previously described (*20*). Protein concentrations were determined by the method of Lowry et al. (*21*), using bovine serum albumin (1 mg/mL standard from PIERCE) as a standard. Spin-labeled fatty acid, 5-SASL, was synthesized as described in ref *22*. Spin-labeled phosphatidylcholine, 5-PCSL, acylated with 5-SASL at the *sn*-2 position was prepared as described in ref *23*. Spin-labeled phosphatidylglycerol, 5-PGSL, and other corresponding spin-labeled phospholipid species were prepared from 5-PCSL by phospholipase D-catalyzed headgroup exchange as described in the same reference. 5-NAPESL was prepared as described in ref *24*, and 5-DGSL was prepared as in ref *25*. Dimyristoyl phosphatidylcholine and dimyristoyl phosphatidylglycerol (DMPC and DMPG) were obtained from Avanti Polar Lipids (Alabaster, AL).

ESR Spectroscopy. Samples for ESR spectroscopy were prepared essentially as described in ref *16* by hydrating the dried lipids with solutions of the proteins in 10 mM Hepes, 5 mM EDTA, 150 mM NaCl, pH 7.4 buffer. The concentration of the protein stock solutions was approximately 8 mg/mL. ESR spectra were recorded on a 9-GHz Bruker EMX EPR spectrometer, with a model ER 041 XK-D microwave bridge. Samples were placed in 50-μL glass capillaries and flame-sealed. The capillaries were placed in a standard 4-mm quartz sample tube containing light silicone oil for thermal stability. The temperature of the sample was maintained constant by blowing thermostated nitrogen gas through a quartz dewar. Spectra were recorded using the following instrumental settings: sweep width, 120 G; resolution, 1024 points; time constant, 20.48 ms; sweep time, 41.9 s; modulation frequency, 100 kHz; modulation amplitude, 1.0 G; and incident power, 5.0 mW. Values of the outer hyperfine splitting, $2A_{max}$, were determined by measuring the difference between the low-field maximum and the high-field minimum.

Attenuated Total Reflectance (ATR) Spectroscopy. Polarized ATR infrared spectra were recorded on a Bruker (Karlsruhe, Germany) IFS-25 Fourier transform spectrometer at a resolution of 4 cm^{-1}. A horizontal ATR accessory from Specac (Orpington, U.K.) was used with a zinc selenide crystal (45° angle of incidence, six reflections). The ATR accessory was modified to seal the sample chamber hermetically from above and to thermostat the cell housing with internally circulating water from a Haake (Karlsruhe, Germany) temperature-controlled bath. The surface of the ATR crystal available for coating by the sample was 8 × 45 mm. A germanium-mounted, wire-grid, linear polarizer (Specac, Orpington, U.K.) was used in the incident beam. Typically, 512 interferograms were co-added and Fourier-transformed after two levels of zero filling and apodization with a Blackman−Harris three-term function.

Samples containing 1 mg of lipid, either DMPG or 1:1 mol/mol DMPG/DMPC, were dried down in a clean glass tube from a 10 mg/mL solution in 3:1 (v/v) $CHCl_3$/MeOH. The dry DMPG lipid film was hydrated with 40 μL of 10 mM Hepes, 5 mM EDTA, pH 7.4 buffer containing 1 M NaCl, whereas the mixed lipids were hydrated with 40 μL of the same buffer containing 150 mM NaCl. The samples were vortexed and subjected to five cycles of freezing (in liquid nitrogen) and thawing (at 37 °C), before being layered on top of a clean zinc selenide ATR crystal. An oriented lipid film was obtained by careful evaporation of the buffer using a continuous stream of dry N_2 gas, followed by overnight vacuum desiccation. Protein stock solutions (∼8 mg/mL) were prepared in 10 mM Hepes, 5 mM EDTA, 150 mM NaCl, pH 7.4 D_2O buffer and were incubated in the refrigerator overnight to allow complete hydrogen−deuterium exchange. The dry lipid film was hydrated directly with a solution containing 100 μg of protein. The sample was hydrated at 35 °C, inside the spectrometer; after 10 min, the temperature was changed to 24 °C. Atmospheric moisture was removed by purging dry nitrogen continuously at a pressure of 1.5 kp/cm^2. After approximately 2−3 h of incubation, ATR spectra were recorded with radiation polarized parallel and perpendicular to the plane of the incident beam. Alignment of the lipid films was checked from the dichroism of the lipid chain CH_2 symmetric and antisymmetric stretch bands (see later).

To determine the dichroic ratio and secondary-structural elements, each spectrum was analyzed using the Peak Fitting Module (PFM) of Origin Pro 7 (Microcal Software, Hampton, MA). If necessary, spectra were smoothed with 11-point Savitsky−Golay smoothing. A local baseline was established, and curve fitting was carried out over the range from 1600 to 1700 cm^{-1}. The intensity ratios of parallel and perpendicular polarization were taken as the ATR dichroic ratio (R), using component intensities obtained from the curve-fitting analysis of the amide I band.

Analysis of Dichroic Ratios and Intensities. The dichroic ratio of the amide I band for a planar β-sheet is given by (*26*)

$$R_I = \frac{E_x^2}{E_y^2} + \frac{2\langle\cos^2\alpha\rangle\langle\sin^2\beta\rangle}{1 - \langle\cos^2\alpha\rangle\langle\sin^2\beta\rangle}\frac{E_z^2}{E_y^2} \quad (1)$$

where α is the inclination of the β-sheet to the normal to the orienting substrate and β is the tilt of the β-strands within the β-sheet. For a partially aligned sample,

$$\langle\cos^2\alpha\rangle = f\langle\cos^2\alpha\rangle_o + (1 - f)/3 \quad (2)$$

where $(1 - f)$ is the fraction unaligned and $\langle\cos^2\alpha\rangle_o$ is referred to the membrane normal.

In fact, the amide I dichroism is determined directly by the orientational distribution of the amide I transition moments. The latter lie in the plane of the sheet, perpendicular to the strands. Therefore, the inclination (ρ) of the

amide I moment, relative to the normal to the orienting substrate, is given simply by

$$\cos \rho = \cos \alpha \sin \beta \tag{3}$$

(see, e.g., ref *26*). The orientational distribution then corresponds to $\langle \cos^2 \rho \rangle = \langle \cos^2 \alpha \rangle \langle \sin^2 \beta \rangle$ in eq 1.

To obtain the true absorbed intensity that reflects relative populations in aligned samples, it is necessary to combine absorbances, $A_{\parallel}$ and $A_{\perp}$, for parallel and perpendicular polarized radiation (*27*). The appropriate admixture of $A_{\perp}$ with $A_{\parallel}$ that allows quantitatively for the spectral dichroism is $A_{\parallel} + (2E_z^2/E_y^2 - E_x^2/E_y^2)A_{\perp}$, in the present geometry. The fractional population of a particular component *j* is therefore given by

$$f_j = \frac{A_{\parallel,j} + \left(2\frac{E_z^2}{E_y^2} - \frac{E_x^2}{E_y^2}\right)A_{\perp,j}}{\sum_j \left(A_{\parallel,j} + \left(2\frac{E_z^2}{E_y^2} - \frac{E_x^2}{E_y^2}\right)A_{\perp,j}\right)} \tag{4}$$

where $A_{\parallel,j}$ and $A_{\perp,j}$ are the integrated absorbances of component *j* that are obtained from band fitting to the parallel and perpendicular polarized spectra, respectively.

The intensities of the infrared electric field components that are used to calculate molecular orientations from dichroic ratios and relative populations from band fitting are obtained from the thick-film approximation. This yields values of $E_x^2/E_y^2 = 0.450$ and $E_z^2/E_y^2 = 1.550$, for a ZnSe ATR crystal (see, e.g., ref *28*).

RESULTS

Interactions with Spin-Labeled Lipids in Phosphatidylglycerol and Phosphatidylcholine Membranes. The perturbation in chain mobility of spin-labeled lipids that is induced by association of wild-type α-synuclein with lipid membranes has been characterized previously by using ESR spectroscopy (*16*). Similar methods are used here to investigate the lipid interactions of mutant and truncated α-synucleins, and of the fibrillar form. Figure 1A shows that addition of the truncated protein decreases the mobility (i.e., increases A_{max}) of 5-PGSL in the fluid membrane phase of DMPG, at temperatures above 23 °C. This behavior is qualitatively similar to that found previously for the wild-type protein interacting with DMPG (*16*). In contrast to the latter, however, the truncated protein produces a detectable perturbation in mobility of 5-PCSL in DMPC membranes, although this is smaller than that with DMPG membranes (see Figure 1B). Removal of the negatively charged C-terminal presumably reduces electrostatic repulsion between the proteins, and this allows them to adsorb also on zwitterionic membranes.

Similar experiments with the A30P and A53T α-synuclein mutants reveal that both are able to interact to some extent with DMPG membranes, but neither evidence any interaction whatsoever with DMPC membranes (data not shown). Information on the relative strengths of the interaction with the mutant proteins is obtained from the dependence of the lipid perturbation on the protein concentration. These data are reported later, in the next subsection.

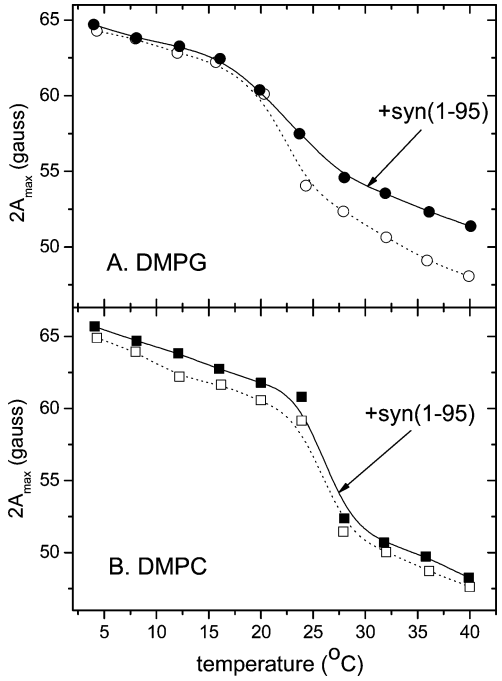

FIGURE 1: Temperature dependence of the outer hyperfine splitting, $2A_{max}$, of 5-position phospholipid spin labels in phospholipid membranes in the presence (● and ■) and absence (○ and □) of truncated α-synuclein(1−95) at a 1:1 wt/wt protein/lipid ratio. (A) 5-PGSL in DMPG bilayer membranes. (B) 5-PCSL in DMPC bilayer membranes.

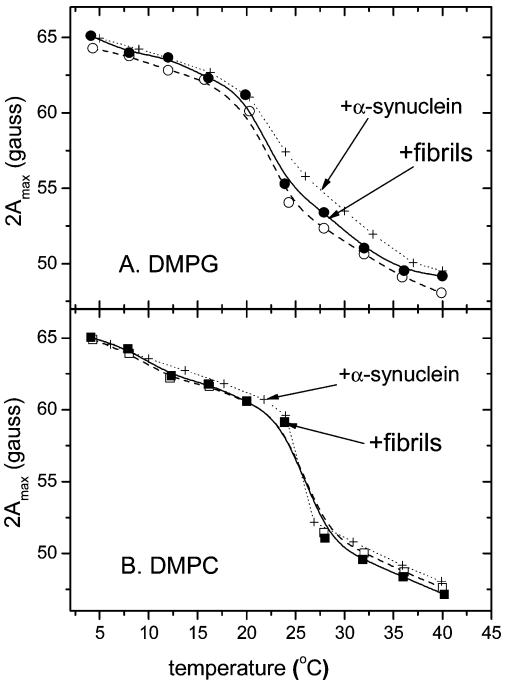

FIGURE 2: Temperature dependence of the outer hyperfine splitting, $2A_{max}$, of 5-position spin labels in lipid membranes in the presence (● and ■) and absence (○ and □) of fibrillar wild-type α-synuclein at a 1:1 wt/wt ratio with respect to the lipid. (A) 5-PGSL in DMPG. (B) 5-PCSL in DMPC. (+) Corresponding data for nonfibrillar wild-type α-synuclein from ref *16*.

Figure 2 gives the temperature dependences of the outer hyperfine splittings, $2A_{max}$, of 5-PGSL in DMPG membranes and of 5-PCSL in DMPC membranes, in the presence and

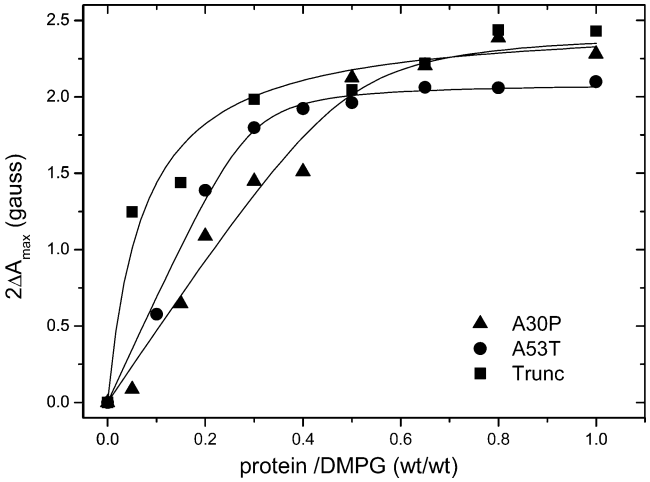

FIGURE 3: Dependence of the increase, $2\Delta A_{max}$, in outer hyperfine splitting of the 5-PGSL phosphatidylglycerol spin label on the protein/lipid ratio in DMPG membranes at 30 °C; (■) truncated α-synuclein(1−95), (●) A53T mutant, and (▲) A30P mutant.

absence of fibrillar preparations of wild-type α-synuclein. These data provide little indication for a strong interaction of α-synuclein fibrils with either anionic or zwitterionic lipid membranes. The spin-label mobility is the same in the presence and absence of fibrillar α-synuclein for DMPC membranes and is rather similar with and without fibrils for DMPG membranes, throughout the gel-phase, transitional, and fluid-phase temperature regimes. (Typical uncertainties in $2A_{max}$ are ±0.2 G, i.e., comparable to the size of the symbols in Figure 2.) In contrast, the interaction of soluble (i.e., nonfibrillar), wild-type α-synuclein with DMPG membranes produces a significant decrease in lipid chain mobility. This is indicated by the data from ref *16*, which are given by crosses and dotted lines in Figure 2. (Note that an error in the field scan by a factor ×1.2 in ref *16* is corrected in Figure 2.)

Protein−Lipid Titration. Figure 3 gives the increase in outer hyperfine splitting, $2A_{max}$, of spin-labeled phosphatidylglycerol (5-PGSL) with increasing concentrations of truncated α-synuclein(1−95) or of the A53T and A30P mutants, added to DMPG membranes. The high concentrations that, for sensitivity reasons, must be used in an ESR experiment preclude accurate determination of association constants. Nevertheless, a tighter association of the truncated protein, relative to the mutants, is evidenced by the much steeper initial slope for the increase in $2A_{max}$ with added protein. Normalized to previous results for wild-type α-synuclein (*16*), the initial slopes in Figure 3 are given by ratios: 0.9, 0.3, and 0.2 for truncated, A53T, and A30P α-synucleins, respectively, relative to the initial slope for wild-type α-synuclein, when the protein/lipid ratio is expressed in terms of moles.

Selectivity of Lipid−Protein Interaction. The selectivity of interaction of different lipids with truncated and mutant α-synucleins bound to DMPG was determined by using probe amounts of 5-position spin-labeled lipids. Figure 4 shows the ESR spectra of the different spin-labeled phospholipids, 5-PXSL, and of spin-labeled stearic acid, 5-SASL, in fluid bilayer membranes of DMPG, in the presence and absence of a saturating amount of truncated α-synuclein(1−95). Also included in Figure 4 are spectra of spin-labeled *N*-acyl phosphatidylethanolamine, 5-NAPESL, in which the

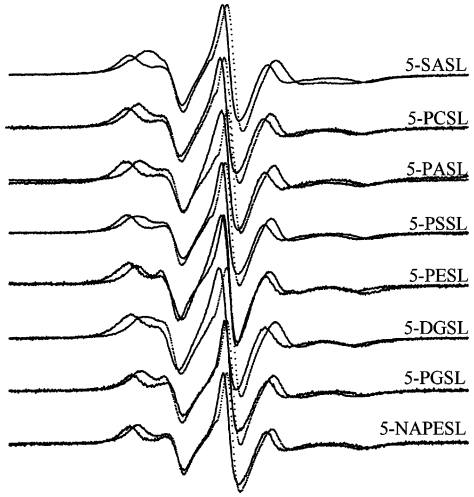

FIGURE 4: ESR spectra of different 5-position spin-labeled lipid species (5-PXSL, 5-SASL, 5-NAPESL, and 5-DGSL, as indicated) in fluid-phase DMPG bilayer membranes in the presence (—) and absence (···) of truncated α-synuclein(1−95) at a 1:1 wt/wt protein/lipid ratio. T = 38 °C; scan width = 120 G.

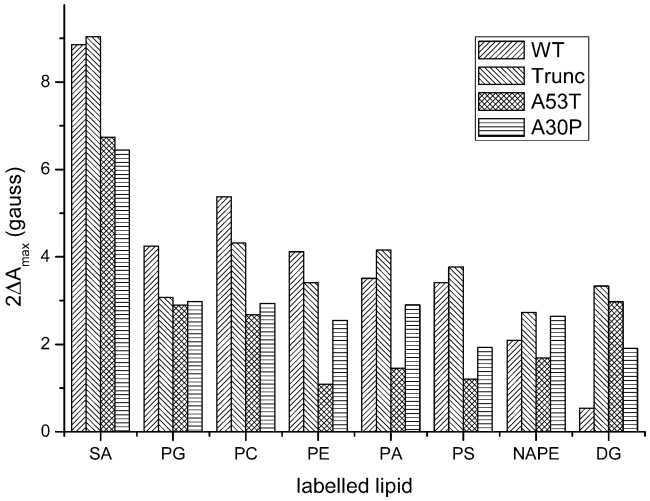

FIGURE 5: Increase, $2\Delta A_{max}$, in outer hyperfine splitting of different 5-position spin-labeled lipid species in DMPG membranes at 38 °C, in the presence of a 1:1 wt/wt ratio with respect to DMPG of (from left to right) wild-type α-synuclein (acute hatch), truncated α-synuclein(1−95) (oblique hatch), A53T mutant (diamond hatch), or A30P mutant (horizontal hatch). SA, stearic acid; PG, phosphatidylglycerol; PC, phosphatidylcholine; PE, phosphatidylethanolamine; PA, phosphatidic acid; PS, phosphatidylserine; NAPE, *N*-acyl phosphatidylethanolamine; DG, diacylglycerol.

spin label is at the 5-position of the *N*-acyl chain, and of spin-labeled diglyceride, 5-DGSL, which lacks the phospholipid headgroup but the spin label is still at the 5-position of the *sn*-2 chain.

For all spin-labeled lipids tested, and for the different modified α-synucleins, the outer hyperfine splitting, $2A_{max}$, is at least somewhat greater for the protein-bound membranes than for the free lipid membranes. The increase in $2A_{max}$ reflects the selectivity of interaction with different lipid headgroups and also the different strengths of lipid interactions with the different forms of α-synuclein. Figure 5 gives the increase, $2\Delta A_{max}$, in outer hyperfine splitting for the various protein-bound membranes, for each of the spin-labeled lipids tested. The most pronounced patterns of selectivity and the largest degrees of perturbation (i.e., largest values of $2\Delta A_{max}$)

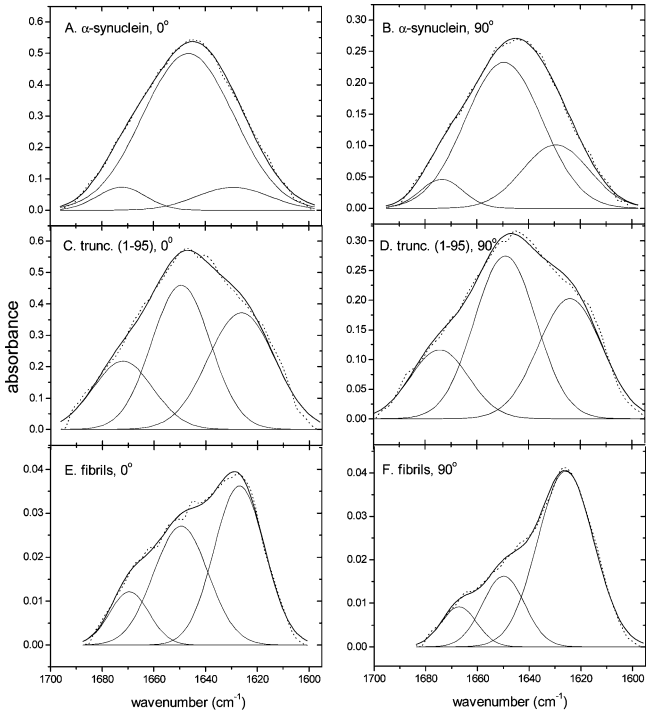

FIGURE 6: Amide I region in the polarized ATR infrared spectra from α-synuclein in 10 mM Hepes, 5 mM EDTA, 150 mM NaCl, pH 7.4 D_2O-buffer solution at 24 °C; (•••) experimental spectrum, and (—) envelope from band fitting. Left-hand panels (A, C, and E) radiation polarized parallel (∥), and right-hand panels (B, D, and F) radiation polarized perpendicular (⊥), and right-hand panels to the plane of incidence; (A and B) wild-type α-synuclein in solution, (C and D) truncated α-synuclein(1−95) in solution, and (E and F) fibrillized wild-type α-synuclein. The components obtained from band-fitting analysis are shown below each experimental spectrum.

are for the wild-type and truncated proteins. With the exception of 5-PGSL, the perturbations of the anionic lipid probes by truncated α-synuclein are greater than by the wild-type protein. This can be attributed to removal of C-terminal negative charges in the truncated protein.

Polarized Infrared Spectroscopy of Wild-Type α-Synuclein. Parts A and B of Figure 6 show the amide I region from the ATR infrared spectrum of wild-type α-synuclein alone in D_2O buffer. The band shape is very similar for both polarizations of the incident radiation, and the dichroic ratio, $R_{tot} = A_{\parallel}/A_{\perp} \approx 2.1$ (on the basis of the total areas of the bands), is characteristic of an isotropically distributed species ($R_{iso} = 2$ in the thick-film approximation). The amide I spectrum of the protein in solution consists predominantly of an extremely broad band centered around 1644 cm^{-1}, such as is typical for natively unfolded proteins in D_2O (*29*, *30*).

Parts A and B of Figure 7 show the amide I spectra of wild-type α-synuclein in the presence of DMPG bilayer membranes that are deposited on the ATR crystal. Relative to the protein in solution, the center of gravity of the amide I band is shifted to higher wavenumber (maximum at 1646 cm^{-1}) and a slight shoulder appears on the low-frequency flank. The overall dichroism of the band, $R_{tot} \approx 1.9$, however, is not significantly less than that for an isotropic distribution. Parts C and D of Figure 7 show similar spectra for wild-type α-synuclein interacting with DMPC membranes containing 50 mol % of DMPG. The low-frequency shoulder is more pronounced than in parts A and B of Figure 7, but the

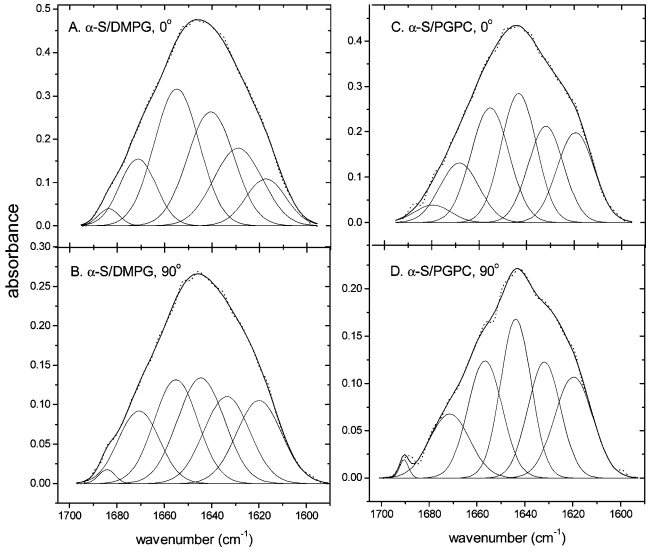

FIGURE 7: Amide I region in the polarized ATR infrared spectra from membrane-bound wild-type α-synuclein in 10 mM Hepes, 5 mM EDTA, 150 mM NaCl, pH 7.4 D_2O-buffer at 24 °C; (•••) experimental spectrum, and (—) envelope from band fitting. Upper panels (A and C) radiation polarized parallel, and lower panels (B and D) radiation polarized perpendicular, to the plane of incidence; (A and B) wild-type α-synuclein and aligned DMPG membranes (in buffer containing 1 M NaCl), and (C and D) wild-type α-synuclein and aligned 1:1 mol/mol DMPC/DMPG membranes. The components obtained from band-fitting analysis are shown below each experimental spectrum.

Table 1: Band Fitting of the Polarized ATR Spectra from the Amide I Band of Wild-Type or Truncated (1−95) α-Synuclein Associated with Hydrated Bilayers of DMPG or 1:1 mol/mol DMPG/DMPC[a]

	DMPG		DMPG/DMPC	
protein	position (cm^{-1})[b]	normalized area (%)[c]	position (cm^{-1})[b]	normalized area (%)[c]
wild type	1619	16	1619	17
	1631	17	1632	25
	1642	22	1645	27
	1654	25	1658	24
	1669	17	1671	6
	1683	2	1678	1
truncated	1621	34	1619	32
	1637	18	1632	10
	1648	19	1643	25
	1658	16	1657	19
	1672	12	1673	11
	1685	3	1686	3

[a] See Figures 7 and 8 for wild-type and truncated α-synuclein, respectively. [b] Secondary-structural assignments in D_2O are typically (*30*): intermolecular β-sheet, 1615−1625 cm^{-1}; antiparallel β-sheet, 1630−1636 cm^{-1} (s) and 1670−1680 cm^{-1} (w); irregular, 1640−1648 cm^{-1}; and α-helix, 1646−1655 cm^{-1}. [c] Normalized areas of the individual components are obtained by using eq 4.

overall dichroism is similar. The results of band fitting are shown beneath the experimental spectra for the membrane-bound protein, in parts A−D of Figure 7. Quantitative data for the relative component intensities, calculated according to eq 4, are given in Table 1. Typical uncertainties in the band fitting are ∼10−20% of the reported values, where the larger uncertainty is associated with the overlapping components in the center of the amide I band.

Polarized Infrared Spectroscopy of Truncated α-Synuclein. Parts C and D of Figure 6 show the amide I region from the

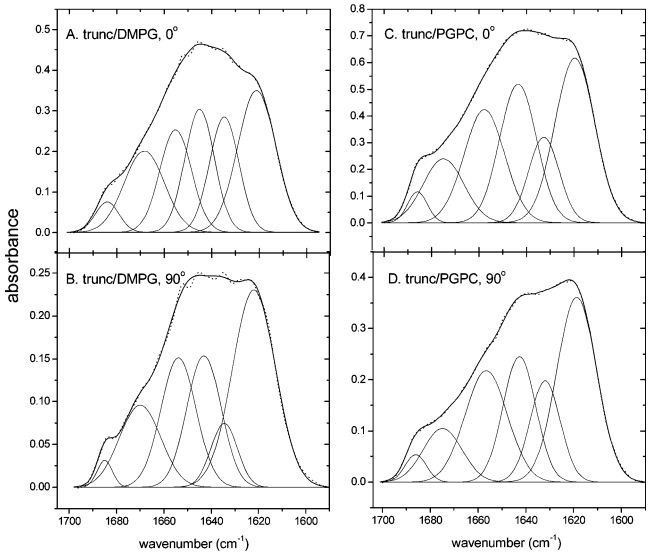

FIGURE 8: Amide I region in the polarized ATR infrared spectra from membrane-bound truncated α-synuclein(1−95) in 10 mM Hepes, 5 mM EDTA, 150 mM NaCl, pH 7.4 D_2O-buffer at 24 °C; (•••) experimental spectrum, and (—) envelope from band fitting. Upper panels (A and C) radiation polarized parallel, and lower panels (B and D) radiation polarized perpendicular, to the plane of incidence; (A and B) truncated α-synuclein(1−95) and aligned DMPG membranes (in buffer containing 1 M NaCl), and (C and D) truncated α-synuclein(1−95) and aligned 1:1 mol/mol DMPC/DMPG membranes. The components obtained from band-fitting analysis are shown below each experimental spectrum.

ATR infrared spectrum of truncated α-synuclein(1−95) alone in D_2O buffer. In comparison with the spectrum of the wild-type protein in parts A and B of Figure 6, the amide I band shape is considerably more asymmetric, with a very pronounced shoulder at ca. 1625 cm^{-1} on the low-frequency side. This indicates the presence of some secondary structure, most likely β-sheet, in at least part of the sample. The formation of such secondary-structural elements presumably results from elimination of the electrostatic repulsion between the negatively charged C-terminal sections of the native protein. These secondary-structural elements must be aligned, relative to the ATR crystal, to some extent, because the dichroic ratio of the overall amide I band is $R_{tot} = 1.75$, which is significantly less than that for an isotropic distribution. (Uncertainties in R_{tot} are less than ± 0.2 for proteins in the absence of lipid but can vary by up to ± 0.3, depending upon conditions affecting membrane alignment, in the presence of lipid.)

Parts A and B of Figure 8 show the amide I spectra of truncated α-synuclein(1−95) in the presence of DMPG bilayer membranes. Relative to the protein in solution (parts C and D of Figure 6), the low-field shoulder at 1625 cm^{-1} is enhanced and a corresponding high-frequency shoulder appears at ca. 1680 cm^{-1}. Absorption peaks at such positions in the amide I band are characteristic of antiparallel β-sheets (see, e.g., ref *26*). The band shape differs considerably between the parallel and perpendicular polarizations, and the dichroic ratio of the total amide I band is $R_{tot} = 1.7$. Parts C and D of Figure 8 show similar spectra for truncated α-synuclein interacting with 1:1 mol/mol DMPC/DMPG membranes. Relative to parts A and B of Figure 8, the spectral components corresponding to antiparallel β-sheets have increased intensity, although the dichroic ratio for the entire amide I band is $R_{tot} = 2.0$. The results of band fitting are shown beneath the experimental spectra for the membrane-bound protein, in Figure 8. Quantitative data for the relative component intensities, calculated according to eq 4, are given in Table 1.

Table 2: Effective Tilt, θ (deg), of the Lipid Chains in Aligned Membranes of DMPG and 1:1 mol/mol DMPG/DMPC at 24 °C, in the Presence of Wild-Type (WT) and Truncated (trunc) α-Synuclein

lipid	protein	θ_s (2849 cm^{-1})[a]	θ_{as} (2918 cm^{-1})[b]
DMPG	WT	38°	37°
DMPG	trunc(1−95)	33°	35°
DMPG/DMPC	WT	32°	33°
DMPG/DMPC	trunc(1−95)	32°	36°

[a] Deduced from the dichroism of the CH_2 symmetric stretch band at 2849 cm^{-1}. [b] Deduced from the dichroism of the CH_2 antisymmetric stretch band at 2918 cm^{-1}.

Lipid Chain Dichroism and Orientational Order. The degree of alignment of the lipid membranes in the presence of the wild-type and truncated proteins can be gauged from the dichroism of the CH_2 symmetric and antisymmetric stretch bands in the polarized infrared spectra (see, e.g., ref *31*). Table 2 gives the effective tilt angles of the lipid chains, relative to the substrate normal. Essentially consistent values for θ are obtained from the symmetric and antisymmetric stretch bands. In the fluid phase, at 24 °C, θ is an effective value that corresponds to the mean order parameter of the individual chain segments that are undergoing rotational isomerism. The values in Table 2 are comparable to those obtained in other fluid lipid membranes (*31*), indicating that the samples are reasonably well-aligned.

Polarized Infrared Spectroscopy of Fibrillar α-Synuclein. Parts E and F of Figure 6 show the amide I region from the ATR infrared spectrum of a fibrillar preparation of wild-type α-synuclein in D_2O buffer. Also shown in parts E and F of Figure 6 are the spectral components obtained by fitting the amide I band at the two polarizations. The spectra contain a major peak at ca. 1626 cm^{-1} that corresponds to β-sheet structures [$\nu_\perp(\pi,0)$ mode]. The low-intensity shoulder at ca. 1670 cm^{-1} at the high-frequency edge of the amide I band likely represents the $\nu_{||}(0,\pi)$ mode that is characteristic of antiparallel β-sheets (*30*, *32*), with possible contributions from β-turns. The amide I band shape of the fibrillar preparations differs greatly between the parallel and perpendicular polarizations. Evidently, the fibrils are aligned on the ATR substrate. The dichroic ratio of the entire band is $R_{tot} = 1.2$ and that of the 1626 cm^{-1} β-sheet component is $R_I = 1.0$. The latter represents 60% of the total integrated intensity (calculated from eq 4), which increases to 62% upon including the high-frequency partner band at ca. 1670 cm^{-1}.

Polarized ATR spectra of either DMPG or 1:1 mol/mol DMPC/DMPG hydrated with a suspension of wild-type α-synuclein fibrils in buffer has very little intensity in the amide I region (data not shown). Not only do the fibrils not interact strongly with the lipid surfaces, but also they presumably are unable to enter the interlamellar aqueous space between the multibilayers to any appreciable extent.

DISCUSSION

The aggregation of α-synuclein is believed to play a critical role in the neurodegeneration that occurs in the common α-synucleinopathies. We previously used ESR to

study the association of wild-type α-synuclein with lipid membranes (*16*). Here, we further exploit ESR spectroscopy, in addition to polarized infrared spectroscopy, to compare the membrane interaction of wild-type α-synuclein with that of the more aggregation-prone mutants A30P and A53T, and the C-terminally truncated α-synuclein(1−95) peptide.

Lipid Interactions of Mutants and Fibrils. The perturbation of the mobility of spin-labeled lipids provides a sensitive means to probe lipid interactions with the different mutant α-synuclein species. The results of Figure 3 indicate that the strength of interaction with anionic phosphatidylglycerol membranes lies in the order: wild type ≈ truncated > A53T > A30P. This is in qualitative agreement with previous findings that the two disease-related mutant forms are able to bind to negatively charged lipid membranes (*6*, *7*, *14*). At high protein/lipid ratios, the lipid perturbation by the A53T and A30P mutants is comparable to that induced by the truncated (and wild-type) proteins (see Figure 3). At low protein/lipid ratios, only the truncated protein induces a perturbation comparable to that of wild-type α-synuclein, as is indicated by the ratio of the initial slopes in the titration.

Alone the truncated α-synuclein(1−95) is found to interact to any extent with zwitterionic phosphatidylcholine membranes. Removal of electrostatic repulsion between the acidic C-terminal domains of the bound protein must account for at least part of this nonvanishing affinity. However, titrating the wild-type protein to acidic pH does not induce any ESR-detectable interaction with phosphatidylcholine (data not shown). C-terminally truncated α-synuclein accumulates in pathological brain tissue and is able to seed full-length α-synuclein (*33*). Thus, binding to phosphatidylcholine, the major phospholipid of mammalian membranes, may facilitate aggregation of α-synuclein in membrane environments not otherwise favoring aggregation of the full-length protein.

The lack of interaction of the A53T and A30P mutants with phosphatidylcholine is fully in-line with their reduced affinity for phosphatidylglycerol membranes. Fibrils of wild-type α-synuclein also do not interact with phosphatidylcholine membranes but additionally display very little affinity for bilayers of phosphatidylglycerol (see Figure 2), in agreement with the results of Volles et al. (*14*). In fact, the ATR studies reveal that α-synuclein fibrils most probably cannot enter the aqueous interlamellar spaces between stacked phospholipid membranes. This is of potential relevance to prefibrillar aggregates at presynaptic nerve endings, because soluble nonpenetrant polymers are able to exert a local osmotic stress that enhances membrane−membrane interactions (*34*).

Lipid Selectivity of Mutants. Perturbations in the pattern and extent of lipid selectivity are also a feature of the mutant α-synucleins. The lipid selectivities reported in Figure 5 are for the association of spin-labeled lipids at probe amounts with the α-synuclein variants that are prebound to DMPG membranes. They therefore reflect local features of the lipid−protein interaction with individual lipids within the membrane and may differ from the bulk lipid requirements for surface binding of the protein (*35*, *36*). Such selectivities determine the in-plane distribution of lipids in the presence of the bound protein, rather than the binding equilibrium between free and membrane-associated protein.

As in previous analysis of the wild-type protein (*16*), we use a model for the selectivity in which the spin-labeled lipids compete for specific sites, with relative association constants,

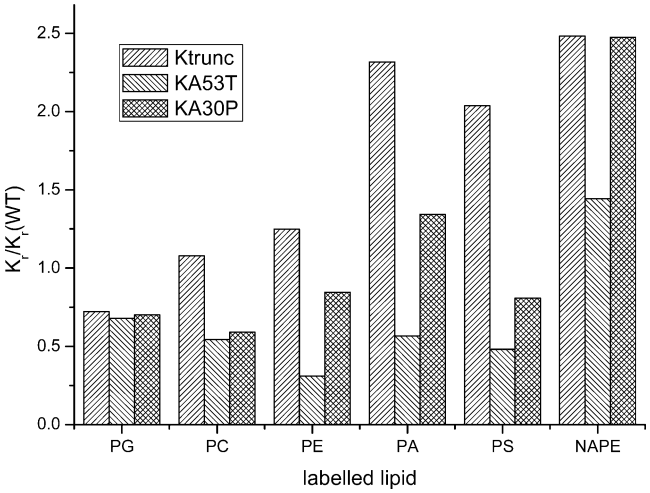

FIGURE 9: Relative association constants, K_r, for different spin-labeled lipids interacting with truncated α-synuclein(1−95) (acute hatch), A53T mutant (oblique hatch), or A30P mutant (diamond hatch), in DMPG membranes. PG, phosphatidylglycerol; PC, phosphatidylcholine; PE, phosphatidylethanolamine; PA, phosphatidic acid; PS, phosphatidylserine; NAPE, *N*-acyl phosphatidylethanolamine. Effective values of K_r, for each spin-labeled lipid, are calculated from eq 5 as described in the text and are normalized to the corresponding values, K_r(WT), for the wild-type protein.

K_r (*35*). Relative to phosphatidylglycerol (PG), the association constants are then related to the increase, $2\Delta A_{max}$, in the outer hyperfine splitting by

$$\frac{K_r}{K_r^{PG}} = \frac{\Delta A_{max}^{o}/\Delta A_{max}^{PG} - 1}{\Delta A_{max}^{o}/\Delta A_{max} - 1} \qquad (5)$$

It is assumed that there is rapid exchange of the lipid between free and bound sites and that the intrinsic value of ΔA_{max} for the bound species is ΔA_{max}^{o}. The latter is not known, but the value of ΔA_{max} for 5-SASL, which is the largest value measured and is very similar for the wild-type and truncated proteins (see Figure 5), provides an approximate (lower) estimate. With this assumption, values of K_r/K_r^{PG} can be derived from eq 5. Making the additional assumption that the values of K_r^{PG} are the same for all proteins (because DMPG is the host lipid in each case) then leads to values of K_r for each protein that are normalized to those for wild-type α-synuclein. These normalized values are presented in Figure 9.

In nearly all cases (except NAPESL), the affinities of the different lipids for the mutant α-synucleins are less than those for the wild-type protein. On the other hand, except for PG, the affinity of each lipid for truncated α-synuclein exceeds that for the wild-type protein. Increased affinity of anionic lipids for the truncated protein is attributable, at least in part, to removal of the negatively charged C-terminal domain of α-synuclein. Increased affinity of α-synuclein(1−95) for zwitterionic lipids correlates, correspondingly, with the ability of the truncated protein to interact with DMPC bilayers. By contrast, the similarities in K_r for 5-PGSL interacting with the truncated and mutant proteins (Figure 9), as opposed to the differences in strength of binding to DMPG (Figure 3), reflect the difference between the in-plane association of lipids with the bound protein and the binding reaction of the protein to the membrane surface, which was referred to above.

It is already known that anionic micelles and lipid vesicles stimulate the aggregation of α-synuclein (*37*). The recently demonstrated stimulation of the aggregation of full-length α-synuclein by C-terminally truncated α-synuclein in solution (*33*) therefore may be potentiated by the favored vesicle binding of this peptide, because we find that this interaction initiates β-folded structure in the truncated monomer, whereupon additional aggregation may be seeded.

Secondary Structure. Wild-type α-synuclein in solution contains little significant content of secondary-structural elements and is considered natively unfolded. The truncated protein that lacks the C-terminal section is mostly unfolded but possesses up to 16% β-sheet content at the concentrations in solution used for IR spectroscopy. Fibrillar full-length α-synuclein, on the other hand, consists of approximately 62% antiparallel β-sheet (see Figure 6).

Both wild-type and truncated β-synucleins evidence increased secondary-structural content upon binding to negatively charged membranes composed of DMPG alone or the 1:1 mol/mol DMPG/DMPC mixture. In each case, (antiparallel) β-sheet structure is present in the membrane-bound protein. Circular dichroism spectra have previously revealed the formation of predominantly α-helical structure (60−80%) upon binding monomeric α-synuclein to lipid membranes (*5*, *6*). The two curved α-helices formed by binding α-synuclein to detergent micelles comprise 60% of the residues of the full-length protein, spanning the whole of the repeat region (*13*). On the other hand, protofibrillar α-synuclein (which binds very tightly to lipid vesicles) is a β-sheet-rich structure (*14*). Estimation of the precise α-helical content of the membrane-bound protein from the present infrared spectra is hampered by the possibility of residual unordered structure, because the latter contributes a broad band that completely overlaps the contributions from α-helix in the amide I region (see parts A and B of Figure 6). With this caveat in mind, the results of band fitting for membrane-bound wild-type and truncated α-synuclein are summarized in Table 1.

All membrane-bound proteins have an appreciable component at the low-frequency edge of the amide I region (ca. 1619 cm^{-1}) that is accompanied by a low-intensity component at the high-frequency edge ($\geq$1680 cm^{-1}). These outer components are characteristic of intermolecular antiparallel β-sheets, of the type found in aggregated and denatured proteins (see, e.g., refs *38* and *39*), or at the edge of β-sheets as in concanavalin A (*29*). The proportion of this β-sheet component is higher for truncated α-synuclein(1−95) (35−37%) than for the wild-type protein (18%), when bound to DMPG or DMPG/DMPC (see Table 1). This could be explained by a greater tendency of the truncated protein to aggregate on the membrane surface, which results from removal of charge repulsion between the C-terminal segments. Recently, this has been found for the truncated protein in solution (*33*).

In addition to the components at the outer extremes, the amide I bands of the bound proteins also contain appreciable intensity at the standard position for β-sheets or extended chains, in the region of 1631−1637 cm^{-1}. These components are accompanied by weaker intensity in the higher frequency region at 1669−1673 cm^{-1} that is expected for antiparallel β-sheets. From Table 1, it is seen that up to 21−30% of the intensity for the truncated protein and up to 31−34% for the wild-type protein are attributed to this β-sheet component. Almost certainly, these estimates also include contributions from β-turns to the intensity at higher frequency (see, e.g., ref *30*). Possibly, the appearance of β-structure upon association with membranes arises from the formation of protofibrils (*14*) or the lower order oligomers observed associated with cellular lipid droplets (*9*), and this is potentiated by the high surface density of the bound protein. It is perhaps significant in this context that the recent NMR structure of micelle-bound α-synuclein contains two short stretches of extended chain/turn structure: one in the linker between the two helices and the other immediately before the mobile C-terminal tail (*13*). Together, these make up 9% of the total residues and may form nucleation sites for the formation of a more extensive β-structure at the membrane surface.

The band intensity fitted at 1654−1658 cm^{-1} in Figures 7 and 8 corresponds to the standard position for α-helices. This contributes ca. 19−25% to the total intensity. A comparable intensity is fitted with a band at 1642−1648 cm^{-1} that corresponds to the position of the broad band for the unfolded protein at 1644 cm^{-1} in parts A and B of Figure 6. Together, these two fitted components constitute 35−44% of the amide band intensity for the truncated protein and 47−51% for the native protein (see Table 1). These possibly may be taken as upper estimates for the α-helical content of the membrane-bound proteins. On the whole, these estimates are lower (and those of β-sheet are correspondingly higher) for protein bound to DMPG membranes than for protein bound to the DMPG/DMPC mixed membranes. This might be attributable to the higher charge density on the DMPG membranes.

Dichroism and Protein Orientation. The dichroism of the fibrillar preparation (see parts E and F of Figure 6) suggests that the fibrils are partially oriented at the surface of the ATR crystal. Application of eq 1 leads to a composite value of $\langle\cos^2\alpha\rangle\langle\sin^2\beta\rangle = 0.15$ for the orientation of the β-sheet and strands. This corresponds to an effective tilt $\rho_{eff} = 67°$ of the amide I transition moments (which lie in the plane of the sheet, perpendicular to the strands), relative to the normal to the ATR crystal. In the cross-β conformation, the amide I transition moments are oriented preferentially parallel to the fiber axis (*40*, *41*). Thus, as expected, the fibrils are oriented preferentially along the surface of the ATR crystal.

The spectra of the membrane-bound proteins that are given in Figures 7 and 8 exhibit differences in dichroism throughout the band shape. This is most pronounced for the low-frequency (1619 cm^{-1}) component of the truncated protein associated with DMPG/DMPC membranes (parts C and D of Figure 8). For the latter, the dichroic ratio yields a value of $\langle\cos^2\alpha\rangle\langle\sin^2\beta\rangle = 0.30$, which corresponds to an effective tilt $\rho_{eff} = 57°$ of the amide I transition moments relative to the normal to the ATR plate. Somewhat similar values are generally obtained for the β-sheet components of the other protein/lipid systems. The large degree of overlap in the α-helix region of the spectrum unfortunately precludes the determination of accurate dichroic ratios for this component of the secondary structure.

CONCLUSION

Lower order oligomers or protofibrils of α-synuclein are considered the neurodegenerative effector molecules in the

synucleinopathies, but their genesis in biological systems is unclear. Disease-causing missense mutations and C-terminal truncations have been demonstrated to stimulate the aggregation of α-synuclein. However, our data demonstrate that the mutants and C-terminal truncations may employ different proaggregatory mechanisms when analyzed in systems containing phospholipid membranes, and thus better resembling cells, as compared to aqueous buffer systems. Both mutants display a lower affinity for phospholipid membranes, as compared to wild-type α-synuclein. In contrast, the C-terminally truncated peptide possesses a higher affinity and, importantly, also a wider range of selectivity for nonacidic phospholipids. This suggests that C-terminally truncated peptides, demonstrated to be present in inclusions of sporadic cases of Parkinson's disease (*42*), target membranes and thereby increase their already high proaggregatory potential. On the other hand, the missense mutations seem to exert their pathogenic effect in solution, which follows also from the A30P mutant being compromised in its vesicle-binding activity (*9*, *18*). The *β*-folded structure is a hallmark for nucleation-competent oligomers; thus, our demonstration here of a significant amount of *β*-folded structure in membrane-bound α-synuclein species suggests that the proaggregatory mechanisms may rely on membrane-induced formation of such nucleation-competent structures. Investigations of Parkinson's disease models based on missense mutants may thus be further away from the sporadic cases that they are meant to model, and the use of C-terminal truncated α-synuclein molecules might represent a better choice.

ACKNOWLEDGMENT

We thank Frau B. Angerstein for synthesis of spin-labeled lipids.

NOTE ADDED AFTER ASAP PUBLICATION

There was an error in the Discussion in the *Secondary Structure* section, last sentence of the first paragraph, in the version published ASAP February 8, 2006. Instead of 6% antiparallel *β*-sheet, there should be 62% antiparallel *β*-sheet. The corrected version was published ASAP February 10, 2006.

REFERENCES

1. Duda, J. E., Lee, V. M. Y., and Trojanowski, J. Q. (2000) Neuropathology of synuclein aggregates: New insights into mechanisms of neurodegenerative diseases, *J. Neurosci. Res. 61*, 121−127.
2. Polymeropoulos, M. H., Lavedan, C., Leroy, E., Ide, S. E., Dehejia, A., Dutra, A., Pike, B., Root, H., Rubenstein, J., Boyer, R., Stenroos, E. S., Chandrasekharappa, S., Athanassiadou, A., Papapetropoulos, T., Johnson, W. G., Lazzarini, A. M., Duvoisin, R. C., Di Iorio, G., Golbe, L. I., and Nussbaum, R. I. (1997) Mutation in the α-synuclein gene identified in families with Parkinson's disease, *Science 276*, 2045−2047.
3. Kruger, R., Kuhn, W., Muller, T., Woitalla, D., Graeber, M., Kosel, S., Przuntek, H., Epplen, J. T., Schols, L., and Riess, O. (1998) Ala30Pro mutation in the gene encoding α-synuclein in Parkinson's disease, *Nat. Genet. 18*, 106−108.
4. Zarranz, J. J., Alegre, J., Gomez-Esteban, J. C., Lezcano, E., Ros, R., Ampuero, I., Vidal, L., Hoenicka, J., Rodriguez, O., Atares, B., Llorens, V., Tortosa, E. G., del Ser, T., Munoz, D. G., and de Yebenes, J. G. (2004) The new mutation, E46K, of α-synuclein causes Parkinson and Lewy body dementia, *Ann. Neurol. 55*, 164−173.
5. Davidson, W. A., Jonas, A., Clayton, D. F., and George, J. M. (1998) Stabilization of α-synuclein secondary structure upon binding to synthetic membranes, *J. Biol. Chem. 273*, 9443−9449.
6. Perrin, R. J., Woods, W. S., Clayton, D. F., and George, J. M. (2000) Interaction of human α-synuclein and Parkinson's disease variants with phospholipids−Structural analysis using site-directed mutagenesis, *J. Biol. Chem. 275*, 34393−34398.
7. Jo, E. J., McLaurin, J., Yip, C. M., St. George-Hyslop, P., and Fraser, P. E. (2000) α-Synuclein membrane interactions and lipid specificity, *J. Biol. Chem. 275*, 34328−34334.
8. Narayanan, V., and Scarlata, S. (2001) Membrane binding and self-association of α-synucleins, *Biochemistry 40*, 9927−9934.
9. Cole, N. B., Murphy, D. D., Grider, T., Rueter, S., Brasaemle, D., and Nussbaum, R. L. (2002) Lipid droplet binding and oligomerization properties of the Parkinson's disease protein α-synuclein, *J. Biol. Chem. 277*, 6344−6352.
10. George, J. M., Jin, H., Woods, W. S., and Clayton, D. F. (1995) Characterization of a novel protein regulated during the critical period for song learning in the zebra finch, *Neuron 15*, 361−372.
11. Segrest, J. P., Jones, M. K., de Loof, H., Brouillette, C. G., Venkatachalapathi, Y. V., and Anantharamaiah, G. M. (1992) The amphipathic helix in the exchangeable apolipoproteins: A review of secondary structure and function, *J. Lipid Res. 33*, 141−166.
12. Eliezer, D., Kutluay, E., Bussell, R., Jr., and Browne, G. (2001) Conformational properties of α-synuclein in its free and lipid-associated states, *J. Mol. Biol. 307*, 1061−1073.
13. Ulmer, T. S., Bax, A., Cole, N. B., and Nussbaum, R. L. (2005) Structure and dynamics of micelle-bound human α-synuclein, *J. Biol. Chem. 280*, 9595−9603.
14. Volles, M. J., Lee, S.-J., Rochet, J.-C., Shtilerman, M. D., Ding, T. T., Kessler, J. C., and Lansbury, P. T., Jr. (2001) Vesicle permeabilization of protofibrillar α-synuclein: Implications for the pathogenesis and treatment of Parkinson's disease, *Biochemistry 40*, 7812−7819.
15. Volles, M. J., and Lansbury, P. T., Jr. (2002) Vesicle permeabilization by protofibrillar α-synuclein is sensitive to Parkinson's disease-linked mutations and occurs by a pore-like mechanism, *Biochemistry 41*, 4595−4602.
16. Ramakrishnan, M., Jensen, P. H., and Marsh, D. (2003) α-Synuclein association with phosphatidylglycerol probed by lipid spin labels, *Biochemistry 42*, 12919−12926.
17. Lindersson, E., Lundvig, D., Petersen, C., Madsen, P., Nyengaard, J. R., Hojrup, P., Moos, T., Otzen, D., Gai, W. P., Blumbergs, P. C., and Jensen, P. H. (2005) P25 α stimulates α-synuclein aggregation and is co-localized with aggregated α-synuclein in α-synucleinopathies, *J. Biol. Chem. 280*, 5703−5715.
18. Jensen, P. H., Nielsen, M. S., Jakes, R., Dotti, C. G., and Goedert, M. (1998) Binding of α-synuclein to brain vesicles is abolished by familial Parkinson's disease, *J. Biol. Chem. 273*, 26292−26294.
19. Jensen, P. H., Islam, K., Kenney, J., Nielsen, M. S., Power, J., and Gai, W. P. (2000) Microtubule-associated protein 1B is a component of cortical Lewy bodies and binds α-synuclein filaments, *J. Biol. Chem. 275*, 21500−21507.
20. Lindersson, E., Beedholm, R., Højrup, P., Moos, T., Gai, W. P., Hendil, K. B., and Jensen, P. H. (2004) Proteasomal inhibition by α-synuclein filaments and oligomers, *J. Biol. Chem. 279*, 12924−12934.
21. Lowry, O. H., Rosebrough, N. J., Farr, L., and Randall, R. J. (1951) Protein measurement with the Folin phenol reagent, *J. Biol. Chem. 193*, 265−275.
22. Hubbell, W. L., and McConnell, H. M. (1971) Molecular motion in spin-labelled phospholipids and membranes, *J. Am. Chem. Soc. 93*, 314−326.
23. Marsh, D., and Watts, A. (1982) Spin-labeling and lipid−protein interactions in membranes, in *Lipid−Protein Interactions* (Jost, P. C., and Griffith, O. H., Eds.) Vol. 2, pp 53−126, Wiley-Interscience, New York.
24. Swamy, M. J., Ramakrishnan, M., Angerstein, B., and Marsh, D. (2000) Spin-label electron spin resonance studies on the mode of anchoring and vertical location of the *N*-acyl chain in *N*-acylphosphatidylethanolamines, *Biochemistry 39*, 12476−12484.
25. Heimburg, T., Angerstein, B., and Marsh, D. (1999) Binding of peripheral proteins to mixed lipid membranes: Effect of lipid demixing upon binding, *Biophys. J. 76*, 2575−2586.

26. Marsh, D. (1997) Dichroic ratios in polarized Fourier transform infrared for nonaxial symmetry of β-sheet structures, *Biophys. J. 72*, 2710−2718.
27. Marsh, D. (1999) Quantitation of secondary structure in ATR infrared spectroscopy, *Biophys. J. 77*, 2630−2637.
28. Marsh, D. (1999) Spin label ESR spectroscopy and FTIR spectroscopy for structural/dynamic measurements on ion channels, *Methods Enzymol. 294*, 59−92.
29. Byler, D. M., and Susi, H. (1986) Examination of the secondary structure of proteins by deconvoluted FTIR spectra, *Biopolymers 25*, 469−487.
30. Tatulian, S. A. (2003) Attenuated total reflection Fourier transform infrared spectroscopy: A method of choice for studying membrane proteins and lipids, *Biochemistry 42*, 11898−11907.
31. Ramakrishnan, M., Pocanschi, C. L., Kleinschmidt, J. H., and Marsh, D. (2005) Orientation of β-barrel proteins OmpA and FhuA in lipid membranes. Chainlength dependence from infrared dichroism, *Biochemistry 44*, 3515−3523.
32. Miyazawa, T. (1960) Perturbation treatment of the characteristic vibrations of polypeptide chains in various configurations, *J. Chem. Phys. 32*, 1647−1652.
33. Liu, C. W., Giasson, B. I., Lewis, K. A., Lee, V. M., DeMartino, G. N., and Thomas, P. J. (2005) A precipitating role for truncated α-synuclein and the proteasome in α-synuclein aggregation, *J. Biol. Chem. 280*, 22670−22678.
34. Rand, R. P., and Parsegian, V. A. (1989) The hydration forces between phospholipid bilayers, *Biochim. Biophys. Acta 988*, 351−376.
35. Sankaram, M. B., De Kruijff, B., and Marsh, D. (1989) Selectivity of interaction of spin-labelled lipids with peripheral proteins bound to dimyristoylphosphatidylglycerol bilayers, as determined by ESR spectroscopy, *Biochim. Biophys. Acta 986*, 315−320.
36. Sankaram, M. B., and Marsh, D. (1993) Protein−lipid interactions with peripheral membrane proteins, in *New Comprehensive Biochemistry: Protein−Lipid Interactions* (Watts, A., Ed.) Vol. 25, pp 127−162, Elsevier, Amsterdam, The Netherlands.
37. Necula, M., Chirita, C. N., and Kuret, J. (2003) Rapid anionic micelle-mediated α-synuclein fibrillization *in vitro*, *J. Biol. Chem. 278*, 46674−46680.
38. Muga, A., Mantsch, H. H., and Surewicz, W. K. (1991) Membrane binding induces destabilization of cytochrome *c* structure, *Biochemistry 30*, 7219−7224.
39. Heimburg, T., and Marsh, D. (1993) Investigation of secondary and tertiary structural changes of cytochrome *c* in complexes with anionic lipids using amide hydrogen exchange measurements: An FTIR study, *Biophys. J. 65*, 2408−2417.
40. Parker, K. D., and Rudall, K. M. (1957) Structure of the silk of chrysopa egg stalks, *Nature 179*, 905−906.
41. Geddes, A. J., Parker, K. D., Atkins, E. D. T., and Beighton, E. (1968) "Cross β" conformation in proteins, *J. Mol. Biol. 32*, 343−358.
42. Baba, M., Nakajo, S., Tu, P. H., Tomita, T., Nakaya, K., Lee, V. M., Trojanowski, J. Q., and Iwatsubo, T. (1998) Aggregation of α-synuclein in Lewy bodies of sporadic Parkinson's disease and dementia with Lewy bodies, *Am. J. Pathol. 152*, 879−884.

BI052344D